# Discourse on Corrections to the NRLMSISE-00 Atmospheric Density Model

**Matthew P. Wilkins[*], Chris Sabol[†], Paul J. Cefola[‡], Kyle T. Alfriend[§]**

May 28, 2009

## Abstract

Dynamic calibration of the atmosphere is a technique where corrections to atmospheric density models are generated based upon indirect observations of the atmosphere, typically satellite orbital data. Previous work showed that the observability of certain density correction parameters was degraded during periods of low solar activity. Also, the correction coefficient $b_2$, which is tied to the perigee altitude, was determined to be poorly observable. In this work we use different formulations for the density corrections to see if one formulation leads to greater observability properties. We discovered that almost any choice of basis function which relies solely upon altitude will lead to the same observability concerns already addressed in previous work. Also, we have determined that linear basis functions may not be sufficient to capture the true nature of the error correction function.

## Introduction

Mismodeling of the atmosphere remains a persistent and dominant source of error in orbit determination and prediction for low earth orbit (LEO) satellites despite the scientific community's best efforts to construct realistic models of the Earth's upper atmosphere. In over fifty years of progress in space flight, one can still expect no better than $10 - 15\%$ error in the instantaneous estimate of atmospheric density during quiet space weather periods. During active space weather periods, instantaneous errors can approach $80 - 200\%$.[1, 2, 3, 4, 5, 6, 7, 8] Most recently, Bruce Bowman *et al.* claims to achieve better than 10% error in atmospheric density modeling with a newly formulated version of the Jacchia 1970 model that includes new solar flux proxies.[9]

Distinguished Russian scientists Dr. Vasiliy Yurasov and Dr. Andrey Nazarenko have attempted to capture information about the upper atmosphere from a historical archive of Two Line Element sets (TLEs),

Distribution Statement A: Approved for public release; distribution is unlimited. PA# AFRL/DE07-612.

[*]Staff Engineer, Schafer Corporation, Air Force Maui Optical and Supercomputing Center, 550 Lipoa St, Kihei, Maui, HI 96753, Tel: (808) 891 - 7747, Fax: (808) 874 - 1603, mpwilkins@gmail.com

[†]Director, HSAI-SSA, Air Force Maui Optical and Supercomputing Site, 535 Lipoa St, Kihei, Maui, HI 96753, Tel. (808) 874 - 1594

[‡]Consultant in Aerospace Systems, Spaceflight Mechanics, and Astrodynamics, 59 Harness Lane, Sudbury, MA 01776, Tel/Fax: (978) 579 - 9668, cefola@mit.edu [also Research Affiliate, MIT Department of Aeronautics and Astronautics]

[§]TEES Distinguished Chair Professor, Texas A&M University, 701 H.R. Bright Building, Department of Aerospace Engineering, College Station, Texas 77843-3141, Tel: (831) 648 - 1772, Fax: (831) 648 - 1773, alfriend@aero.tamu.edu

which serve as pseudo-observations of the upper atmosphere.[10, 11, 12, 13] In 1999 and 2002, work was done by George Granholm and Sarah Bergstrom who both wrote their M.I.T. Master's theses on the implementation of the Russia DCA theory.[14, 15]

Sequences of TLEs tell us where a space object was, and then we must reconstruct what atmospheric conditions had to have occurred for the satellite to arrive at that position in space and time. By identifying the difference in what the density model said happened versus our observational data of various space object orbits, we are able to construct a correction time series to the model of interest. This is what we call dynamic calibration of the atmosphere (DCA).

Given that our current atmospheric models clearly lack a precise understanding of these sources of change, the challenge then is to extract useful information from observations of space object motion that allows us to compute corrections to our models of the atmosphere. That is to say, we accept our models are inadequate, and we will attempt to compute a global correction to the model that makes up for these inadequacies. The drawback to TLEs as observation data is that they only indirectly measure atmospheric phenomena. Additionally, our most recent efforts have shown that computing corrections to atmospheric density models have many nuances.[16] Because of the particular approach that was chosen, we found that these nuances are due in large part to the proper use and interpretation of the space weather indices that serve as atmospheric model inputs. However, despite this, we have demonstrated that DCA corrections to the NRLMSISE-00 atmospheric density model can reduce scattering in the estimate of the ballistic factor for a LEO space object in the 200 $km$ to 600 $km$ altitude regime by a factor of 3.6.[17]

Clearly, dynamic calibration of the atmosphere has *multiple* benefits. First, we correct our estimate of atmospheric density generated by a given model. Second, we obtain an *a priori* estimate of the error of that model. In that regard, these density corrections give us an idea of which model might be better suited for a particular class of orbits. Third, we obtain a refined estimate of the "true" ballistic factor for a LEO space object.

## Validation and Application of DCA Theory

The current work of Nazarenko and Yurasov constructs a correction to an atmospheric model density via the following formulation:

$$\rho = \rho_{model}\left(1 + \frac{\delta\rho}{\rho_{model}}\right) \tag{1}$$

In order to determine a functional form for $\dfrac{\delta\rho}{\rho_{model}}$, Nazarenko and Yurasov considered that the time rate of change of a space object's orbit period could be expressed as a function of the ballistic factor, atmospheric density, and some function of the orbit elements.

One would like to be able to express the difference between the model density and the true density as a function of particular variables. For instance, altitude, inclination, local apparent solar time, and latitude are all good examples of parameters that we know the atmospheric density is functionally dependent upon. Therefore, one can construct a correction equation as a series of coefficients multiplied by some functional form of the aforementioned parameters, which ultimately can be solved through the least squares process.

$$\frac{\delta\rho}{\rho_{model}}(h_{ij}, t_j) = \left(\frac{\hat{k}_{ij}}{\bar{k}_i}\right) - 1 = \sum_{q=1}^{N} b_q(t_j) f_q(\cdot) \tag{2}$$

where $\hat{k}_{ij}$ is the $j^{th}$ ballistic factor estimate for the $i^{th}$ space object equivalent to $\frac{c_d A}{m}$, $\bar{k}_i$ is the approximate "true" ballistic factor for the $i^{th}$ space object, $f_q(\cdot)$ are basis functions that attempt to impart physical meaning to their associated correction coefficients $b_q(t_j)$. The choice of basis function is largely arbitrary, and some effort was spent analyzing various choices to decide which choice would be "optimal" given the quality and quantity of observation data available to us for processing.

The functional form used to date is shown in Equation 3.

$$\frac{\delta\rho}{\rho_{model}}(h_{ij}, t_j) = \left(\frac{\hat{k}_{ij}}{\bar{k}_i}\right) - 1 = b_1(t_j) + b_2(t_j)\left(\frac{h_{ij} - h_0}{h_1}\right) = b_1(t_j) + b_2(t_j)\left(\frac{h_{ij} - 400}{200}\right) \tag{3}$$

where $b_1$ and $b_2$ are density correction coefficients and $h_{ij}$ is the perigee altitude of the space object. Here the reference altitudes have been set as $h_0 = 400$ and $h_1 = 200$ to center the linear correction about the midpoint of the altitude range of interest (200 $km$ to 600 $km$). Due to the fact that a reference altitude of 400 $km$ is applied, the $b_2$ correction is nullified when the space object passes through 400 $km$ in altitude. Additionally, the linear form gives a factor of $\pm 1$ to $b_2$ at the boundaries of our considered region (200 $km$, 600 $km$). Note that these corrections, while solved for using perigee altitude, are applied based upon instantaneous altitude. For space objects in highly eccentric orbits, the impact of the $b_2$ coefficient is magnified at high altitudes. However, the density at those altitudes is markedly lower. Whether this impacts our orbit prediction capabilities for eccentric orbits has yet to be studied in detail.

In previous work,[18] we have generated corrections to the NRLMSISE-00 atmospheric density model from November 30, 1999 (2451513.5 JD) to November 30, 2003 (2452973.5 JD) using the 16 space objects identified by Yurasov and Nazarenko in their 2004 Phase III Report[19]. Figures 1(a) and 1(b) show the time history of the density corrections produced as part of this effort and referred to as the Wilkins corrections as compared to those generated by Yurasov in previously published work. Clearly, the computed corrections are nearly identical and differences between these corrections can be attributed to minor differences in implementation.[16]

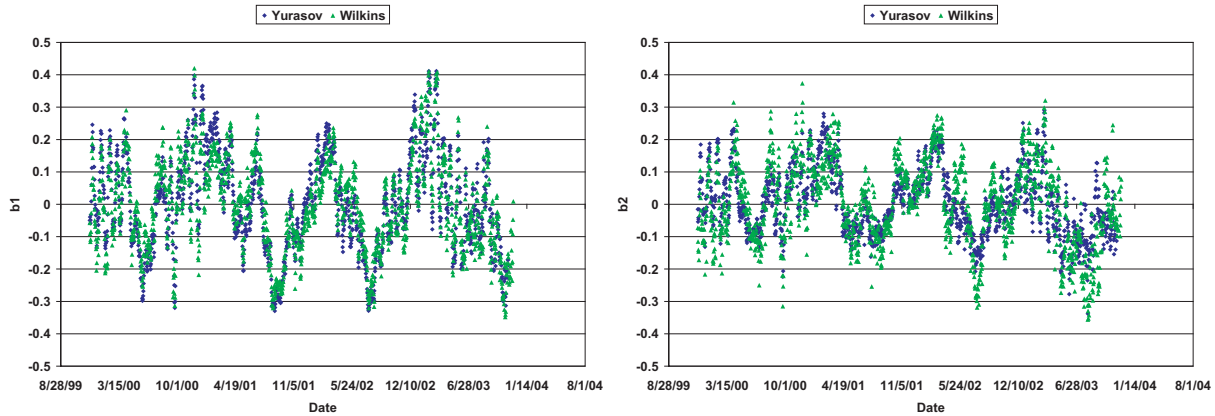


(a) $b_1$ (b) $b_2$

Figure 1: Time history of the $b_1$ and $b_2$ correction coefficients as generated by Wilkins compared to that generated by Yurasov.

## Successive Refinements to Density Corrections

The coefficients $b_1$ and $b_2$ are globally optimal correction coefficients that are tied directly to the choice of basis function. The $b_i$ parameters should not be mistaken for a set of coefficients in a convergent Taylor series, for example. We contend that in order for the residual error estimate to have an expectation of zero, the procedure for determining the corrections to the atmospheric density model should be extended to create a series of vanishing coefficients. This can be effected by altering the correction model to read

$$\rho = \rho_m \prod_{z=1}^{Z} \left(1 + \frac{\delta\rho}{\rho_m}(h_{ij}, t_j)\right)_z = \rho_m \left[1 + \sum_{g=1}^{Z+1} a_g(t_j) f_q(h_{ij})^{g-1}\right] \tag{4}$$

$$\left(1 + \frac{\delta\rho}{\rho_m}(h_{ij}, t_j)\right)_z = \prod_{y=1}^{z} \left[1 + \sum_{q=1}^{2} b_{qy}(t_j) f_q(h_{ij})\right] = \left(\frac{\hat{k}_{ij}}{\bar{k}_i}\right)_{z-1} \tag{5}$$

where $z$ represents a particular level of refinement and $Z$ represents the total number of successive refinements made to our atmospheric density corrections. To illustrate the procedure, write out the first couple of refinement passes. First obtain estimates for the ballistic factors without any sort of corrections added. These estimates, and their associated time average, are denoted with the subscript 0 on the RHS of the equation.

$$\left(1 + \frac{\delta\rho}{\rho_m}(h_{ij}, t_j)\right)_1 = [1 + b_{11}(t_j) + b_{21}(t_j) f_2(h_{ij})] = \left(\frac{\hat{k}_{ij}}{\bar{k}_i}\right)_0 \tag{6}$$

Solve for $b_{11}(t_j)$ and $b_{21}(t_j)$ using the least squares process. These values are fixed for the rest of the procedure. Now, repeat the ballistic factor estimation process but include the first set of corrections to our density model. Obtain a new set of estimates and a new time averaged estimate of the truth and denote them with a subscript 1 on the RHS of the equation.

$$\left(1 + \frac{\delta\rho}{\rho_m}(h_{ij}, t_j)\right)_2 = [1 + b_{11}(t_j) + b_{21}(t_j) f_2(h_{ij})]\,[1 + b_{12}(t_j) + b_{22}(t_j) f_2(h_{ij})] \tag{7}$$

$$= \left(\frac{\hat{k}_{ij}}{\bar{k}_i}\right)_1 \tag{8}$$

where one can solve for $b_{12}(t_j)$ and $b_{22}(t_j)$ using the least squares process. Repeat the entire procedure and include each set of newly generated corrections to the density model in the estimation process. As the process is repeated, the successive refinements to the corrections will become smaller and smaller. We have yet to determine a tolerance on when to stop the iterative refinements. Currently, we have found that three ballistic factor estimation sets, which generates three sets of $b_{1z}$ and $b_{2z}$ corrections, appears to be the maximum number of refinements needed. However, further iteration may still be justified.

In the end, these corrections form a new convergent Taylor series polynomial written about the chosen basis function. The first two coefficients, $a_1$ and $a_2$ are the corrected $b_1$ and $b_2$ coefficients. For the perigee altitude basis functions utilized by Yurasov and Nazarenko, this can be expressed as

$$\rho = \rho_m[1 + a_1(t_j) + a_2(t_j) f_2(h_{ij}) + a_3(t_j) f_2(h_{ij})^2 \tag{9}$$

$$+ a_4(t_j) f_2(h_{ij})^3 + a_5(t_j) f_2(h_{ij})^4 + \cdots] \tag{10}$$

Note that $\rho_m$ is equivalent to $\rho_{model}$ and was abbreviated for clarity.

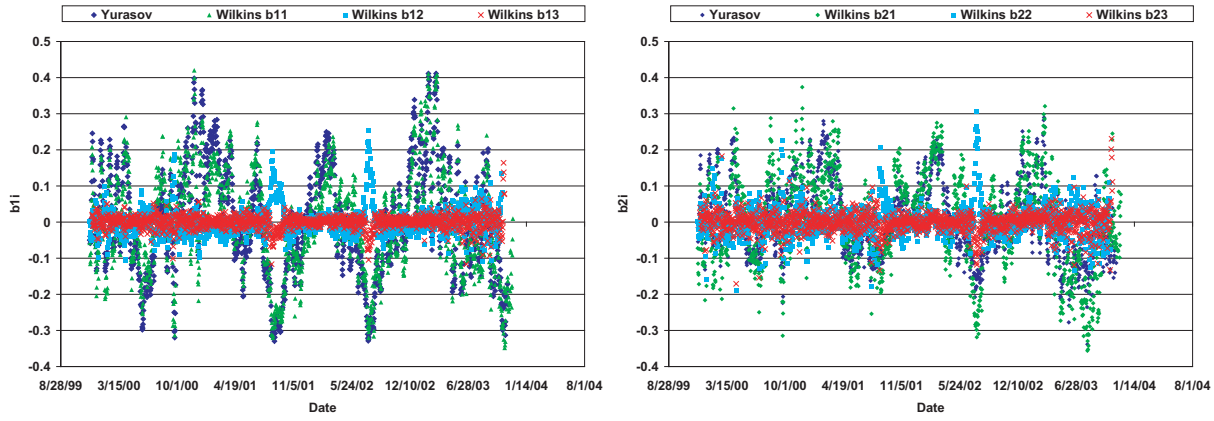


(a) $b_{1i}$ (b) $b_{2i}$

Figure 2: Evolution of $b_1$ and $b_2$ coefficients after successive refinements.

One can analytically compute the series coefficients as functions of the $b_{1i}$ and $b_{2i}$ coefficients determined above. For example,

$$\begin{aligned} a_1 =&(b_{11} + b_{12} + b_{13} + b_{14} + \cdots) + (b_{11}b_{12} + b_{12}b_{13} + b_{11}b_{14} + b_{13}b_{14} + \cdots) \\ &+ (b_{11}b_{12}b_{13} + b_{11}b_{12}b_{14} + b_{11}b_{13}b_{14} + b_{12}b_{13}b_{14} + \cdots) + b_{11}b_{12}b_{13}b_{14} + \cdots - 1 \end{aligned} \tag{11}$$

Notice how each successive refinement is simply an addition to the previous refinement plus cross-correlation terms. This is intuitive and expected. As one computes more and more refinements, the $a_g$ series coefficients should reach some steady state value. The convergence of these terms should be used as the determination for the iterative refinement cut-off tolerance.

Note that when generating the successive passes, one relies on the previous set of corrections as a basis to start from. Because we have not thrown out any outlier data points in the first pass corrections, the successive passes are attempting to correct out these deficiencies - be they physical or mathematical. A careful study would be required to determine whether or not to exclude outliers prior to computing further refinements.

Figures 2(a) and 2(b) show the resulting correction coefficients for each of three stages of refinement. The $2^{nd}$ level of refinement is generated from the ballistic factor estimates resulting from the application of the initial density corrections and so on. The standard deviation of each successive refinement gets smaller and smaller meaning that the corrections to the previous solution for the density coefficients is getting finer. Figure 3 shows the evolution of the standard deviation for both the $b_1$ and $b_2$ coefficients. Notice that the refinements appear to be approaching a steady state value. This indicates that the remaining error will need to be addressed by another method such as generating a series of corrections based upon another quantity like the local apparent solar time.

Figures 4(a) and 4(b) show the comparison with Yurasov's $b_1$ and $b_2$. The remaining terms are shown in Figures 5(a) and 5(b). One can contend that the higher order terms of $a_g$ may be predictors of time periods where our estimates of density corrections are degraded. This is particularly important if you consider that the chosen basis function $f(h_{ij})$ ranges from -1 to +1 over the altitude range of interest which places a heavier weight on the higher order terms when a space object is near 200 $km$ or 600 $km$.

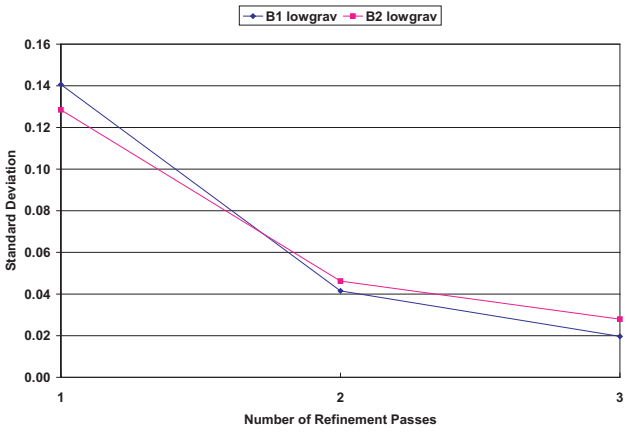


Figure 3: Evolution of the standard deviation in the successively refined $b_1$ and $b_2$ coefficients.

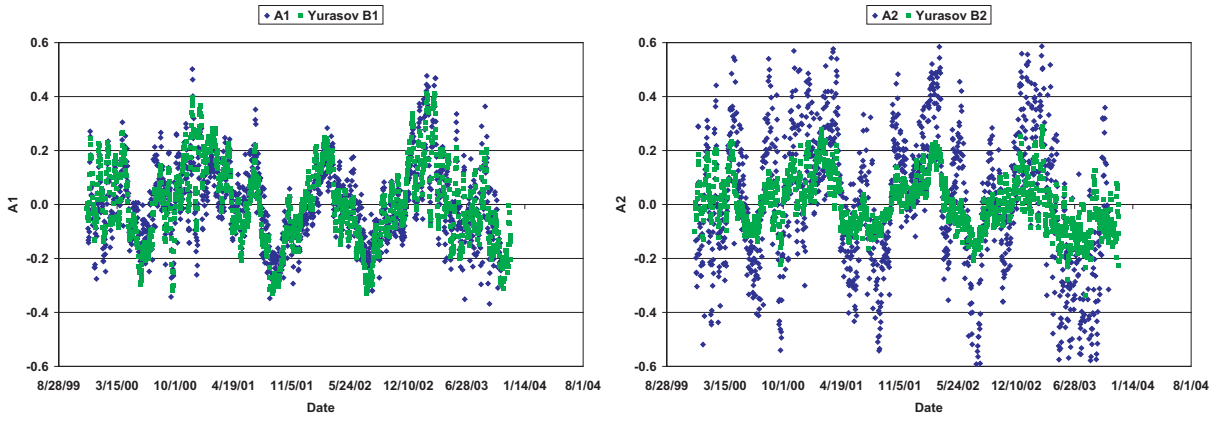


(a) $a_1$ (b) $a_2$

Figure 4: First and second terms of the new density correction polynomial. Yurasov's $b_1$ and $b_2$ coefficients are also plotted for comparison purposes.

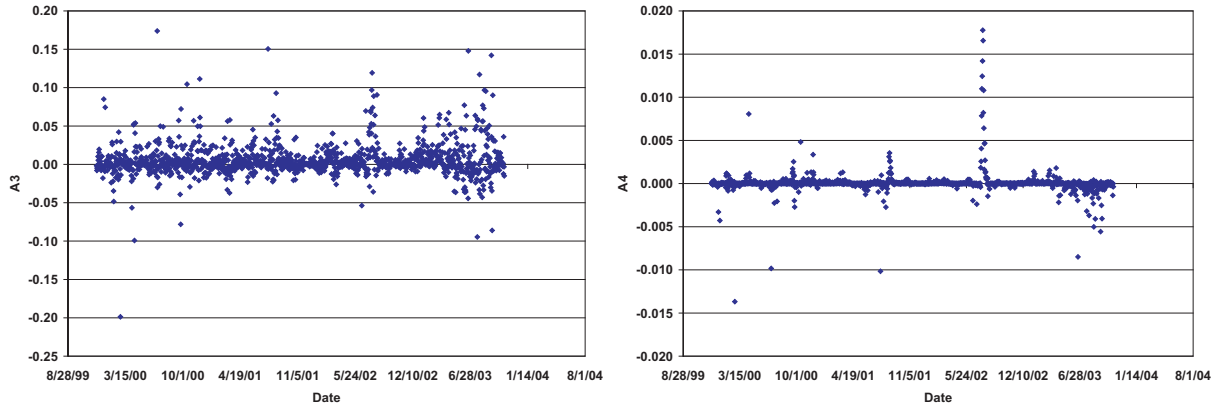


(a) $a_3$ (b) $a_4$

Figure 5: Third and fourth terms of the new density correction polynomial.

Assume for a moment that the $a_g$ coefficients are the "optimal" solution and remove most of the remaining residual error, one would expect that $b_1 \rightarrow a_1$ and $b_2 \rightarrow a_2$ as we increase the number and kind of space objects used to generate the corrections. Therefore, the scatter plots of $a_1$ versus $b_1$ and $a_2$ versus $b_2$ should approach a linear relationship with a slope of 1 if the data sets were identical. The R-squared value indicates how reliable the trendline is with a value close to 1 being the most reliable.

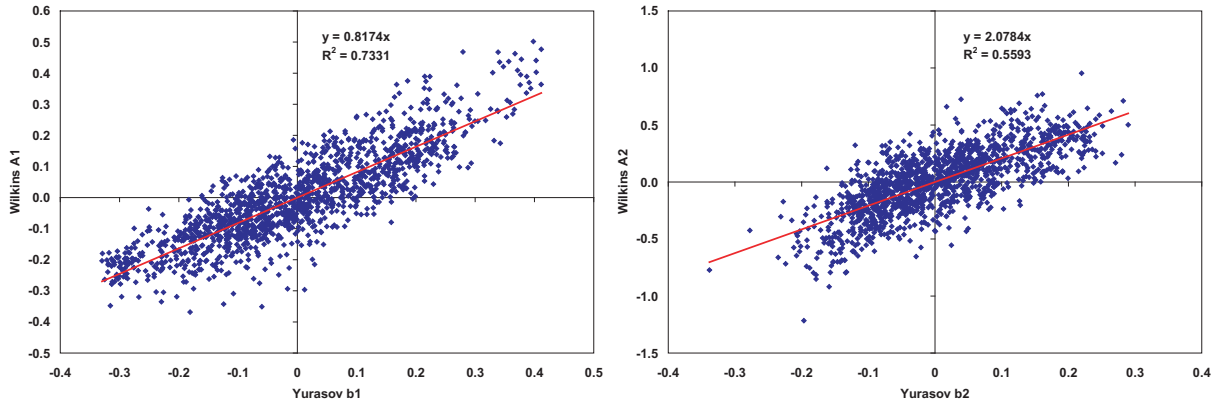


(a) $a_1$ vs $b_1$ (b) $a_2$ vs $b_2$

Figure 6: Scatter plot comparison of Wilkins 16 space object $a_1$ and $a_2$ coefficients versus the $b_1$ and $b_2$ coefficients generated by Yurasov.

Figures 6(a) and 6(b) show a scatter plot comparison of the $a_1$ and $a_2$ coefficients with the corrections generated by Yurasov. In both cases, 16 space objects were utilized. When comparing $a_2$ to $b_2$ the slope is approaching 2, which strongly indicates that the original theory for solving for the $b_2$ coefficient is a suboptimal choice for representation of the density model error in the least squares process. This is consistent

with the observability issues in a companion work.[18]

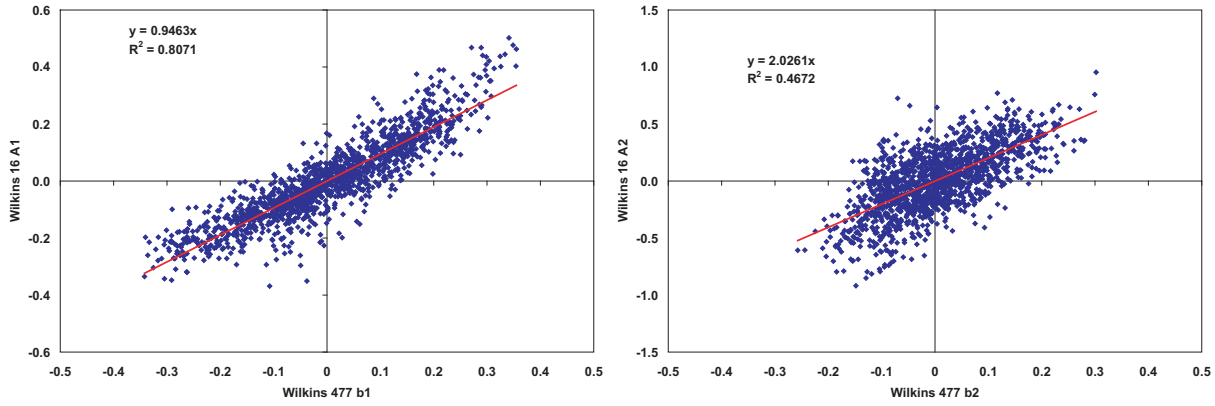


(a) $a_1$ vs $b_1$ (b) $a_2$ vs $b_2$

Figure 7: Scatter plot comparison of Wilkins 16 space object $a_1$ and $a_2$ coefficients versus the 477 space object $b_1$ and $b_2$ coefficients generated by Wilkins.

Similarly, Figures 7(a) and 7(b) compare the $a_1$ and $a_2$ coefficients based upon 16 space objects with the $b_1$ and $b_2$ values from a single pass of the ballistic factor estimation process on 477 space objects. Notice that there is a strong correlation between the 16 space object $a_1$ and the 477 space object $b_1$. This leads us to believe that it is possible to remove unknown sources of error in the ballistic factor estimation process through the successive refinement process using a minimum number of space objects.

## New Insight into the Corrections

In the process of validating the previous work of Nazarenko and Yurasov, we identified some areas of concern regarding how the corrections are generated. As reported previously,[18] we have generated corrections using various size populations that are generally independent of one another. The largest population size was 477 space objects that the Russians used to compute corrections to the GOST and Jacchia-70 atmospheric density models. Figures 8(a) and 8(b) compare these various solutions for the $b_1$ and $b_2$ coefficients generated with various numbers of space objects.

These figures indicate that the $b_1$ density correction is strongly observable and essentially the same regardless of the number of space objects used. Based upon the constituency of the various space object populations, there also does not appear to be any dependence on other orbital parameters such as inclination, eccentricity, or altitude. Looking at the figure for $b_2$, one immediately sees that the solutions vary significantly. In fact, some subsets of satellites produce markedly different solutions than a smaller subset and the next larger population of space objects that also encompasses it. What this indicates is that the $b_2$ coefficient is poorly observable and is highly dependent upon the number of space objects as well as the temporal and spatial distribution of the underlying observations for those objects.

In addition to the concern regarding observability, the way that the $b_1$ and $b_2$ coefficients are derived is somewhat statistically troublesome. This is due to the fact that we are using a direct ratio of the instantaneous solution of the ballistic factor to the so-called "true" ballistic factor. This formulation does

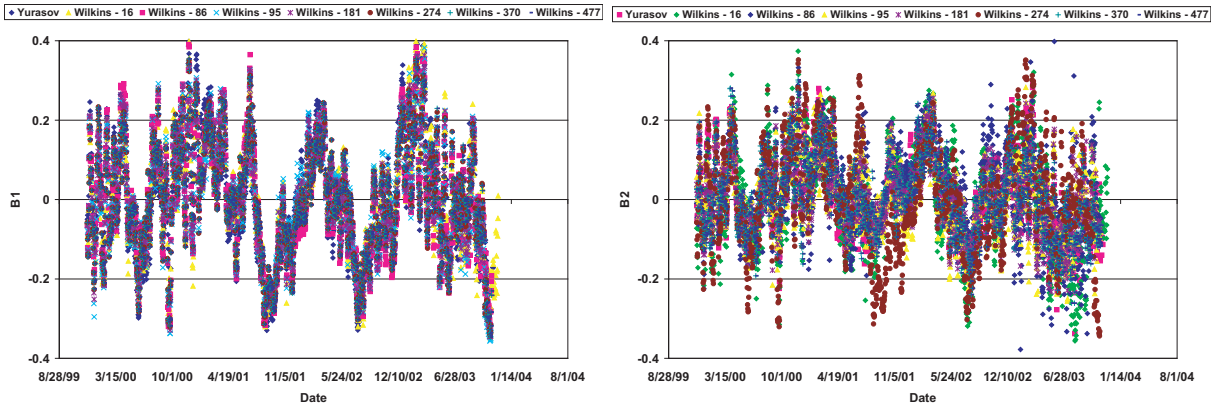


(a) $b_1$ (b) $b_2$

Figure 8: Comparison of various solutions for the $b_1$ and $b_2$ coefficients using a $21 \times 21$ geopotential for the ballistic factor estimation process.

not account for the fact that our estimate of the "true" ballistic factor can be biased nor does it account for the fact that the "true" ballistic factor is statistically still an unknown quantity.

The original theory constructs a relationship between the estimates of the ballistic factors and the correction to the density model as:

$$\left(\frac{\delta\rho}{\rho_{model}}\right) \approx \left(\frac{k_{est}}{k_{true}}\right) - 1 \tag{12}$$

In our previous work,[20] we modified the formulation in Equation 12 to read as follows:

$$\left(\frac{\delta\rho}{\rho_{model}}\right) \approx \left(\frac{2(k_{est} - k_{true})}{k_{est} + k_{true}}\right) \tag{13}$$

where the right hand side is exactly zero if the ballistic factor estimate is equivalent to the truth, hence the absence of the minus one. This new formulation is actually the formula for computing percent difference between two estimated quantities, that is the difference divided by the average which leads to a 2 in the numerator when simplified. Using this formulation, we regenerated the $b_1$ and $b_2$ coefficients based upon the same set of ballistic factor estimates. Table 1 provides the mean and standard deviation of the $b_1$ and $b_2$ coefficients for each case. Figure 9 plots the direct difference in the two solutions. A trendline for the $b_1$ and $b_2$ differences is provided to show a consistent bias between the two solutions. The mean $b_1$ has shifted by 0.0152 and the mean $b_2$ has shifted by 0.0178. This is further evidence of a distinct bias in our original theory and that our corrections to the atmospheric model density could be off in a systemic fashion.

We can compute residual errors for any set of ballistic factor estimates using the various solutions presented in this work. For the sake of illustration, Figure 10 is a plot of the residual errors for each of the 16 space objects in the original study using the newly formulated density corrections based on the full 477 space object case. The residuals appear to be largely white noise and there is not a whole lot of structure to the error. The spikes in the residuals can be attributed to a number of causes, namely outliers in the density correction solution or a given space object passed through a particularly turbulent region of space.

Table 2 shows the residual error computations for various passes of successive refinements using low and high fidelity geopotential models and varying numbers of space objects used to generate the coefficients.

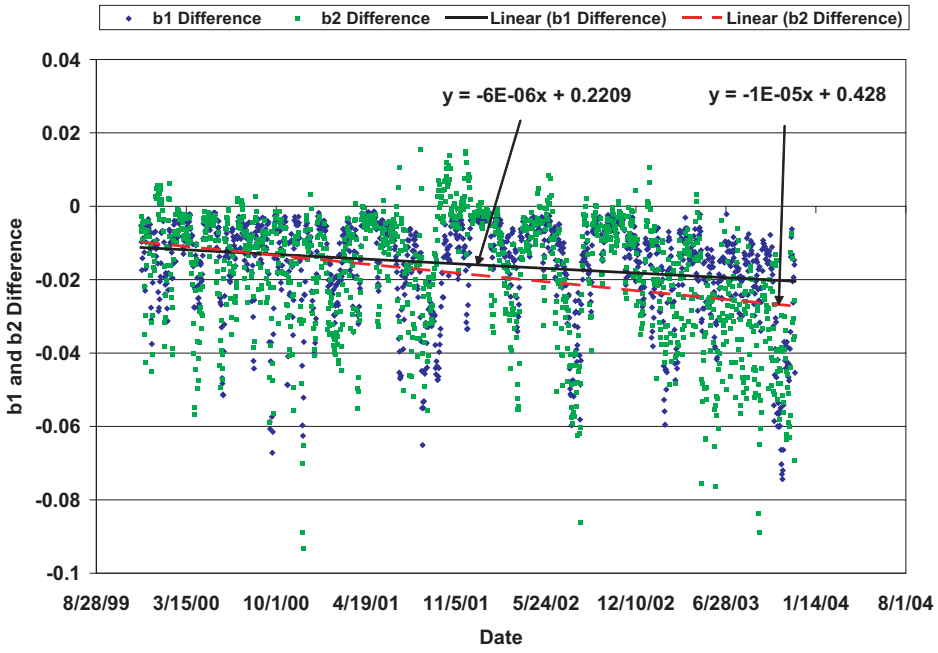


Figure 9: Direct difference of the $b_1$ and $b_2$ coefficients using two different formulations.

Table 1: Statistical comparison of the new formulation for solving for the $b_1$ and $b_2$ coefficients versus the original formulation for the case with 477 space objects.

| | Mean $b_1$ | Std Dev $b_1$ | Mean $b_2$ | Std Dev $b_2$ |
|---|---|---|---|---|
| New Formulation | -1.3685E-02 | 1.4042E-01 | -1.3003E-02 | 9.8231E-02 |
| Original Formulation | 1.5507E-03 | 1.3814E-01 | 4.8081E-03 | 9.5537E-02 |

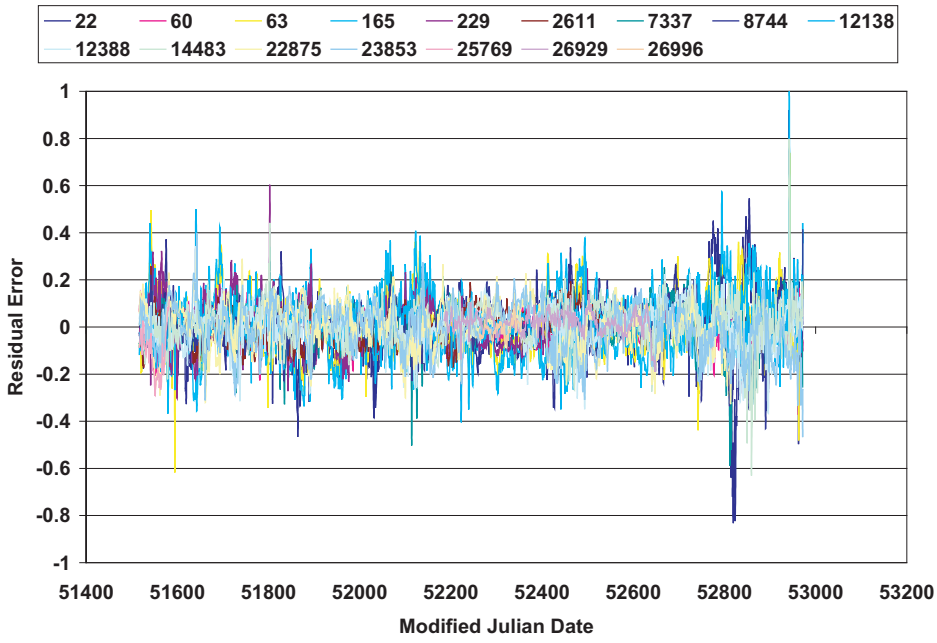


Figure 10: Residual errors for each of 16 space objects in the original study using the newly formulated density corrections based upon the full 477 space objects.

Additionally, the new formulation is applied in various cases to demonstrate the impact on the residual errors. One will notice immediately that the 2nd successive refinement decreases the mean residual error for both the high and low fidelity geopotential despite the fact that the mean residual error for individual space objects as shown in Table 3 remains largely unchanged.

The new formulation reduces the expectation of the residual error by an order of magnitude in all cases except for the full 477 space object case. This could be due to that fact that there is enough space objects such that the statistics are equivalent. Clearly, the new formulation does a better job of minimizing the error in the least square solution process.

Table 2: Statistical data for the residual error in the least squares process resulting from the computation of the density correction using the old and new formulations under the influence of a low- and high-fidelity gravity model. The absolute error that lumps all residuals into a single calculation is presented here.

| Refinement Level | # SO | Applied To | Geopotential | Mean | Std Dev | Var |
|---|---|---|---|---|---|---|
| 1st | 16 | 16 | $21 \times 21$ | -0.01734 | 0.11243 | 0.01264 |
| 1st New Formulation | 16 | 16 | $21 \times 21$ | -0.00131 | 0.10968 | 0.01203 |
| 2nd | 16 | 16 | $21 \times 21$ | -0.00223 | 0.10237 | 0.01048 |
| 1st | 16 | 16 | $50 \times 50$ | -0.01704 | 0.10956 | 0.01200 |
| 1st New Formulation | 16 | 16 | $50 \times 50$ | -0.00137 | 0.10713 | 0.01148 |
| 2nd | 16 | 16 | $50 \times 50$ | -0.00065 | 0.09533 | 0.00909 |
| 1st | 477 | 477 | $21 \times 21$ | -0.00499 | 0.16010 | 0.02563 |
| 1st New Formulation | 477 | 477 | $21 \times 21$ | 0.00609 | 0.16706 | 0.02791 |
| 1st | 477 | 16 | $21 \times 21$ | -0.00456 | 0.09345 | 0.00873 |
| 1st New Formulation | 477 | 16 | $21 \times 21$ | 0.00066 | 0.09592 | 0.00920 |

Most striking are the results from applying the corrections of the 477 space object case to the small subset of 16 space objects. The absolute mean residual error using the corrections generated under the original formulation is virtually unchanged compared to the case where we applied the 16 space object density correction solution to the same set of objects. Furthermore, there is an order of magnitude reduction in the residual error from -0.0158 to 0.0038.

For the case of the 477 space objects, there were 775427 converged ballistic factor estimates out of 815,878 individual fitwindows. Using the original formulation, the absolute mean residual error is -0.03099 with a standard deviation and variance of 0.16639 and 0.027687, respectively. The new formulation reduces the expected value of the residual error for the 477 space object case by a factor of 5.08 which is a significant amount considering the number of individual ballistic factor estimates under consideration. The resulting absolute mean residual error is 0.00609 with a standard deviation and variance of 0.16706 and 0.02791, respectively.

## Breaking the Solution into Distinct Altitude Bands

Using the same ballistic factor estimates from the 477 space object population as before, we decided to break the 200 to 600 $km$ altitude range into four 100 km segments. The $b_1$ and $b_2$ coefficients were computed for each of the four altitude segments. However, only those space objects with perigee heights in the individual

Table 3: Mean residual errors for the individual space objects in the original 16 space object population under the influence of a $21 \times 21$ geopotential. Here the density corrections generated by the 477 space object population is used to compute the residual error for both the original and new formulation for the corrections.

| | Original Formulation | | | New Formulation | | |
|---|---|---|---|---|---|---|
| Satnum | Mean | Std Dev | Var | Mean | Std Dev | Var |
| 22 | -0.031 | 0.134 | 0.018 | 0.008 | 0.136 | 0.019 |
| 60 | -0.011 | 0.060 | 0.004 | 0.002 | 0.060 | 0.004 |
| 63 | -0.028 | 0.113 | 0.013 | 0.009 | 0.113 | 0.013 |
| 165 | -0.032 | 0.143 | 0.021 | 0.021 | 0.145 | 0.021 |
| 229 | -0.045 | 0.094 | 0.009 | -0.014 | 0.092 | 0.008 |
| 2611 | -0.022 | 0.076 | 0.006 | 0.005 | 0.068 | 0.005 |
| 7337 | -0.012 | 0.088 | 0.008 | 0.004 | 0.088 | 0.008 |
| 8744 | -0.008 | 0.090 | 0.008 | 0.007 | 0.089 | 0.008 |
| 12138 | -0.007 | 0.078 | 0.006 | 0.011 | 0.077 | 0.006 |
| 12388 | -0.013 | 0.085 | 0.007 | 0.002 | 0.083 | 0.007 |
| 14483 | -0.003 | 0.092 | 0.008 | 0.013 | 0.089 | 0.008 |
| 22875 | 0.000 | 0.096 | 0.009 | -0.005 | 0.097 | 0.009 |
| 23853 | -0.007 | 0.097 | 0.009 | -0.012 | 0.098 | 0.010 |
| 25769 | -0.105 | 0.106 | 0.011 | -0.102 | 0.104 | 0.011 |
| 26929 | -0.004 | 0.036 | 0.001 | -0.005 | 0.032 | 0.001 |
| Mean | -0.023 | 0.097 | 0.010 | -0.004 | 0.096 | 0.010 |
| Absolute | -0.0158 | 0.098 | 0.010 | 0.0038 | 0.097 | 0.009 |

altitude segments were allowed for the solution of that segment. The reference heights were left the same as in the original case ($h_0 = 400\ km$ and $h_1 = 200\ km$). Ultimately, one would desire to have a piecewise continuous function where the total density correction computed at the boundaries of the segments is identical. In this case, however, the segments are solved independently of one another for simplicity.

Figures 11(a) through 14(b) show the $b_1$ and $b_2$ time histories as compared to the original solution over the entire altitude band. Figures 15(a) and 15(b) compare the various solutions to each other. Please notice that the scale of Figures 11(a) and 11(b) is significantly larger than that of the other plots. This is due to the lack of observational data available in the $200 - 300\ km$ altitude band as evidenced by Figure 16, which shows a comparison of the number of observations during each fit window as broken into the four $100\ km$ altitude bands. This in and of itself indicates that our general solution over the $200 - 600\ km$ probably is not a good representation over the entire range.

Recall that the solution of the $b_1$ coefficient is generally readily observable and, hence, a very stable quantity. At first glance, the plots for $b_1$ in each of the altitude bands above $300\ km$ appear to be very similar. However, to the studied eye, the solution in each altitude band is significantly different and the differences can be tied into the choice of reference height $h_0$. Because the solution for $b_1$ starts to degrade as the distance from the reference altitude increases, we believe that choosing a fictitious reference altitude that has no basis on physical knowledge can impact our understanding of what the density corrections are and what they mean. If we truly wish for the density corrections to have physical meaning and not be affected by mathematical artifices, then we should work toward finding a better choice for the functional

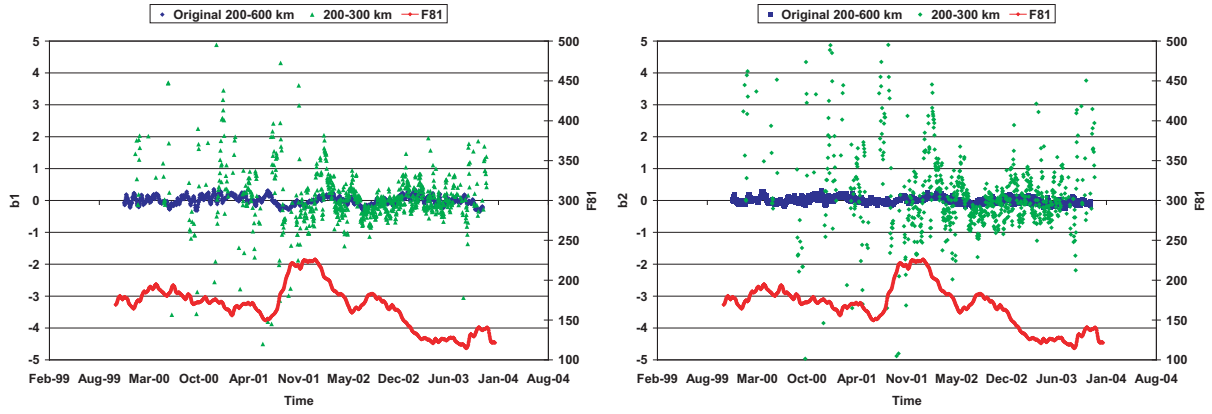


(a) $b_1$ (b) $b_2$

Figure 11: Comparison of the $b_1$ and $b_2$ coefficients from the original solution across the 200 to 600 $km$ altitude range versus the solution obtained over the altitude range 200 to 300 $km$.

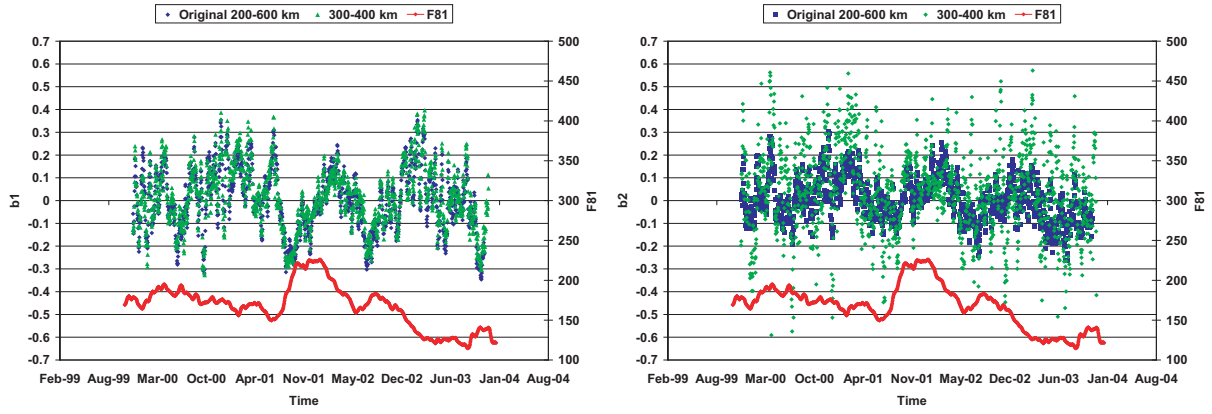


(a) $b_1$ (b) $b_2$

Figure 12: Comparison of the $b_1$ and $b_2$ coefficients from the original solution across the 200 to 600 $km$ altitude range versus the solution obtained over the altitude range 300 to 400 $km$.

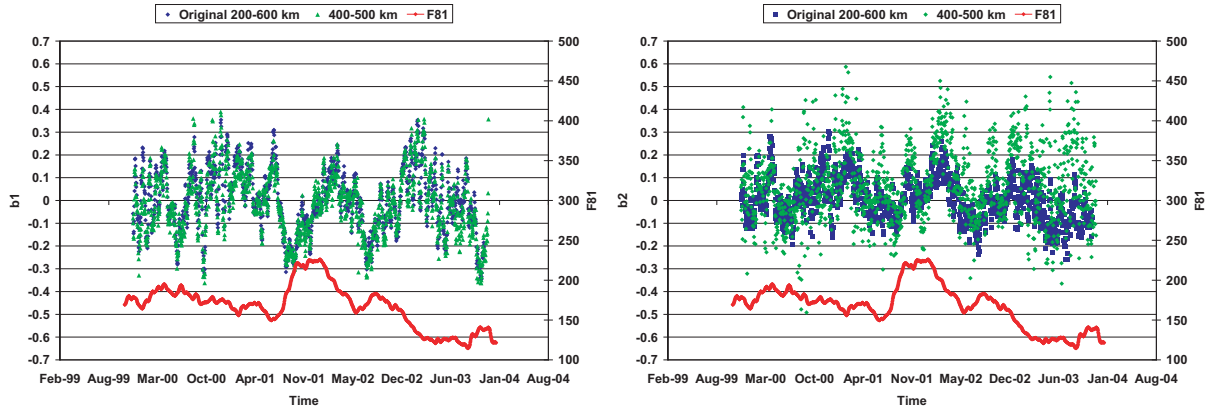


(a) $b_1$ (b) $b_2$

Figure 13: Comparison of the $b_1$ and $b_2$ coefficients from the original solution across the 200 to 600 $km$ altitude range versus the solution obtained over the altitude range 400 to 500 $km$.

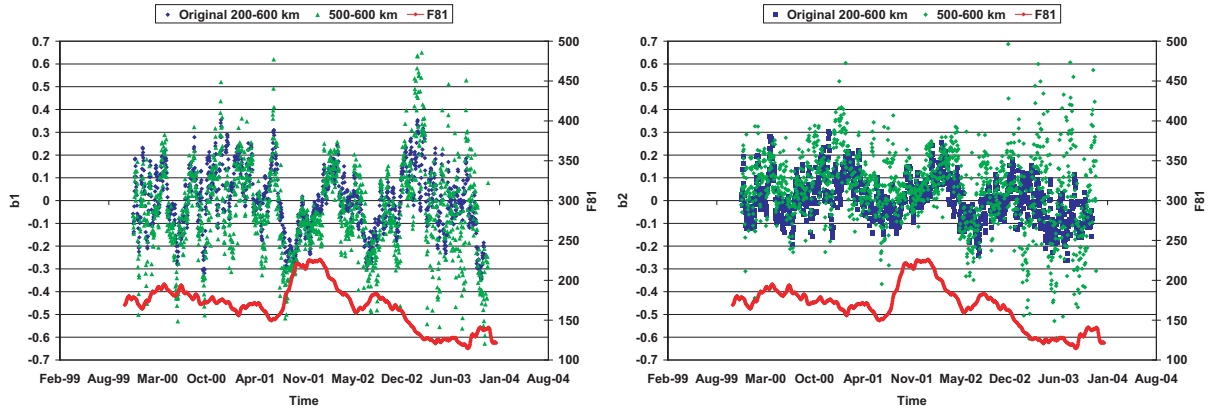


(a) $b_1$ (b) $b_2$

Figure 14: Comparison of the $b_1$ and $b_2$ coefficients from the original solution across the 200 to 600 $km$ altitude range versus the solution obtained over the altitude range 500 to 600 $km$.

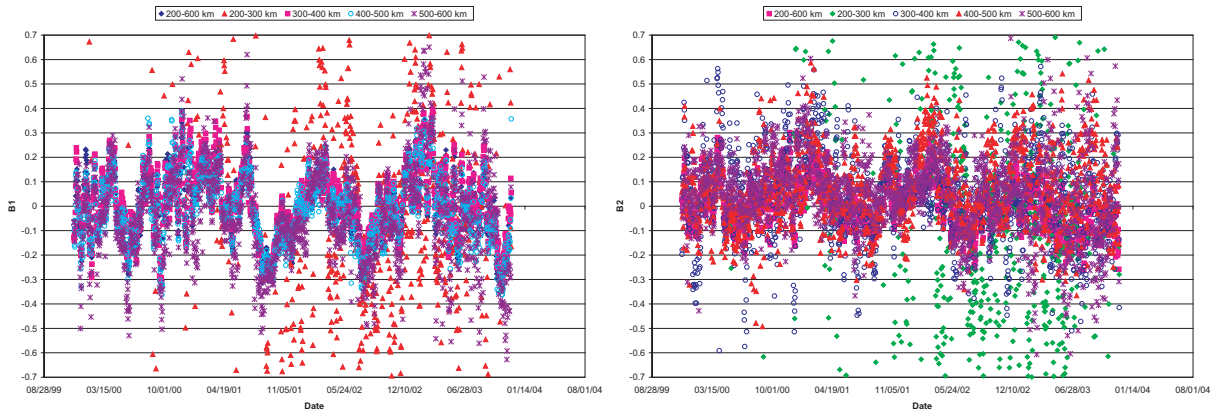


(a) $b_1$ (b) $b_2$

Figure 15: Comparison of various solutions for the $b_1$ and $b_2$ coefficients using a $21 \times 21$ geopotential for the ballistic factor estimation process.

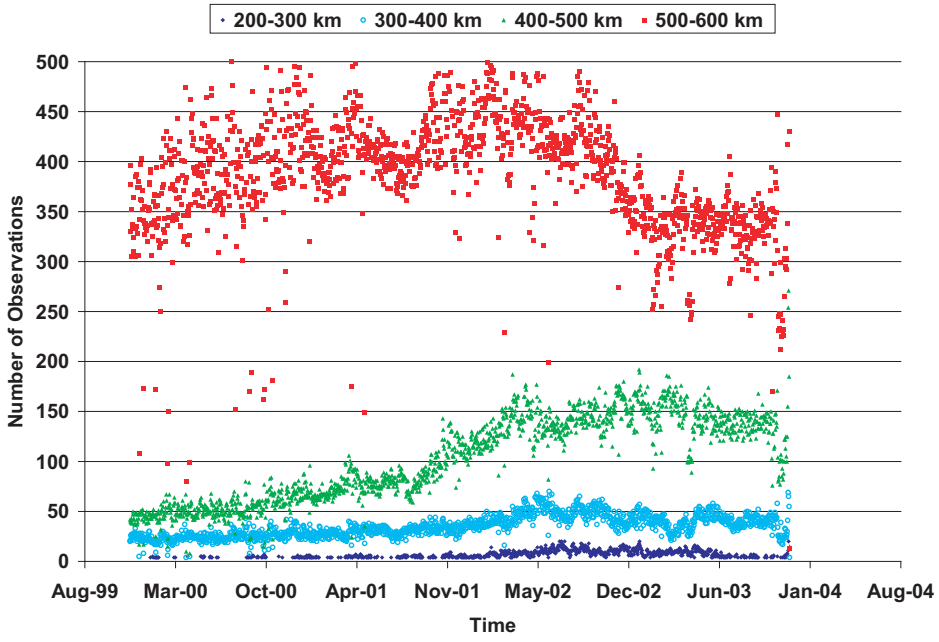


Figure 16: A comparison of the number of observations available during each fitwindow covering four distinct 100 $km$ altitude bands from 200 to 600 $km$.

parameterization of the density corrections.

## Investigating Alternative Formulations

In 1982, Gorochov and Nazarenko investigated functions of altitude, inclination, and argument of the perigee and assumed that they were symmetric fluctuations in the northern and southern hemisphere.[21] The delineated functions include:

$$f_1 = 1 \tag{14}$$

$$f_2 = \frac{h - h_0}{h_1} \tag{15}$$

$$f_3 = \cos\alpha \cos i \tag{16}$$

$$f_4 = \sin\alpha \cos i \tag{17}$$

$$f_5 = \sin^2 i \tag{18}$$

$$f_6 = \cos\alpha \sin^2 i \cos i \tag{19}$$

$$f_7 = \sin\alpha \sin^2 i \cos i \tag{20}$$

$$f_8 = \sin^4 i \tag{21}$$

where $\alpha$ is the right ascension of the perigee, $h$ is the altitude, $h_0$ and $h_1$ are reference altitudes that may be the same or different, and $i$ is the inclination. However, in the end, it was determined that there was only sufficient information to estimate the coefficients of the first two basis functions $f_1$ and $f_2$.[22]

Consider now that we only solve for the first functional formulation $f_1$ (i.e. we only solve for $b_1$). By comparing this solution for $b_1$ to that where we also solve for $b_2$ should indicate how much change in our solution is imparted by solving for a function including altitude. Figure 17 shows a scatter plot comparison of the "$b_1$ only" solution and our previous $b_1$ solution using 477 space objects covering the 200 to 600 $km$ altitude band. A trend line passing through the origin is shown on the plot. If the data sets were identical, then all points would fall on the line, and the line would have a slope of one. The R-squared value is an indicator of the reliability of the trendline, where R-squared values close to 1 are the most reliable.

Clearly, the two solutions for $b_1$ are nearly identical. This result confirms that the $b_1$ coefficient acts as an average correction, or bias, to the density model at a given time and is essentially uncorrelated with the altitude dependent correction coefficient $b_2$. Additionally, this confirms our previous findings that the $b_1$ solution is reasonable and readily observable with a minimum number of space objects. Furthermore, we would like to find a functional form for these corrections that provides consistent solutions regardless of the number and kind of space objects used to generate them.

To that end, we chose different functional forms using perigee altitude to see if one form provides the consistency that we are seeking. Examples of the forms that we looked at are:

$$f(h) = \frac{2(h - h_0)}{h + h_0} \tag{22}$$

$$f(h) = \frac{h}{400} \tag{23}$$

$$f(h) = \frac{400}{h} \tag{24}$$

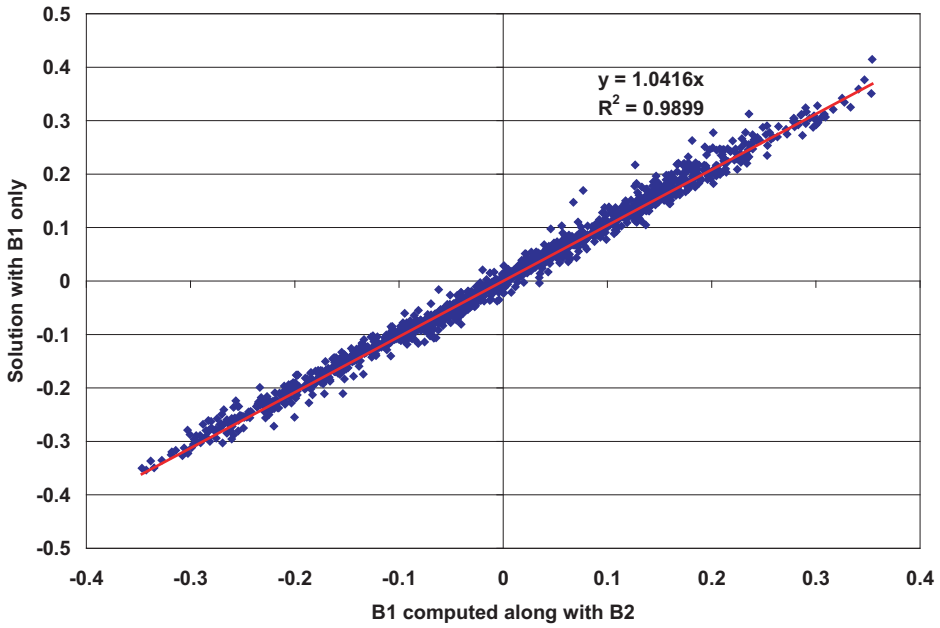


Figure 17: Scatter plot comparison of the "$b_1$ only" solution and our previous $b_1$ solution using 477 space objects covering the 200 to 600 $km$ altitude band.

Figures 18(a) and 18(b) show a representative case where we set the functional form of the altitude correction to the following:

$$f_1 = 1 \tag{25}$$

$$f_2 = \frac{2(h - h_0)}{h + h_0} \tag{26}$$

In each plot, the solution using 477 space objects and an 86 space object subset are shown for comparison. These solutions were generated over the 200 to 600 $km$ altitude range. Clearly, the solutions differ and provide little improvement to the level of consistency over the original formulation. We tried a number of different choices for $f(h)$ and obtained similar results to those shown here. Therefore, if we continue to limit ourselves to using a linearized functional form, we can say that we will have difficulties achieving consistent results for density corrections regardless of the choice of functional form.

## Conclusions and Future Work

Significant progress has been made towards the implementation of procedures for the dynamic calibration of the atmosphere at the Maui High Performance Computing Center. This work has independently validated the Russian DCA theory and has shown conclusively that DCA is a worthwhile endeavor and is able to be replicated on various platforms. While many questions have been answered regarding the implementation of DCA, many more theoretical questions have been posed because the massive computational capabilities

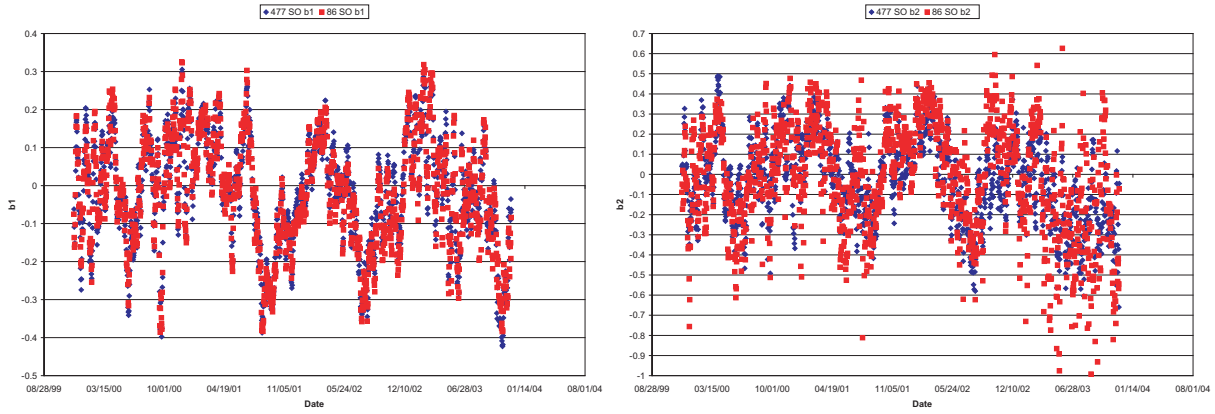


(a) $b_1$ (b) $b_2$

Figure 18: Plot of the $b_1$ and $b_2$ coefficients across the 200 to 600 $km$ altitude range using an alternative formulation.

here have allowed us to push the boundaries of what is conceivable and feasible. This work has only touched the tip of the iceberg in DCA theory and much more investigation is necessary.

We have shown that the $b_1$ coefficient is observable and independent of the number of space objects used as well as their spatial distribution. The $b_2$ coefficient, however, is not readily observable and future work will be required to determine if an alternate formulation for the associated basis function can be found to address this problem. Future work is also necessary to try and use more accurate models for the coefficient of drag to study the impact it has on the computation of the atmospheric density corrections. Furthermore, we need to study if excursions in the ballistic factors that still remain after applying the density corrections can be explained by other parameters such as local apparent solar time or latitude, for example.

We have shown that successive refinements can apply subtle corrections to the first pass density corrections and remove some of the remaining error from the solution. This effort was motivated by the fact that we had non-zero residual errors after a single pass of corrections. As noted in the main text, the successive refinements rely on the previous set of corrections as a basis to start from. Because we have not thrown out any outlier data points in the first pass corrections, the successive passes are attempting to correct out these deficiencies. As future work, we would like to explore the effects of smoothing the individual passes through an optimal Kalman smoother. This will automatically exclude outlying data points in a statistically optimal fashion as well as allow us to fill in any gaps in the density correction time history due to lack of data or lack of converged solutions.

Successive refinements can reduce the computational burden required to determine the density correction coefficients by reducing the number of space objects needed to generate a solution. Furthermore, these refinements have confirmed that the $b_2$ coefficient is difficult to observe as currently formulated. Future work will analyze the total number of refinements, $Z$, required to achieve a desired truncation error in the new correction polynomial.

Based upon the body of work to date, we suggest that it may not be wise to generate a single density correction function across the LEO orbit regime nor should we limit ourselves to solely parameterizing the corrections in terms of perigee altitude. Therefore, we plan to investigate generating a piece-wise continuous correction function that is broken up into smaller altitude bands as well as attempt to use additional

functional parameters such as latitude and local apparent solar time. In this concept, we would only use a ballistic factor estimate from a given fit window to generate a density correction data point if that space object is within the narrow altitude band of interest. In succeeding fit windows, the space object may cross into another altitude band depending upon its eccentricity in which case the ballistic factor estimate would be applied to that new altitude band solution. Likewise, when implementing these corrections into orbit determination and prediction, the choice of correction function would be applied based upon the instantaneous altitude of the space object.

It follows then that out of a set of $N$ space objects, only a small subset would be useful for generating corrections in each altitude band. In previous work we showed that the current formulation requires a minimum number of space objects to get a solution for the $b_1$ parameter and increasing that number does not improve our ability to observe $b_2$. This piece-wise continuous concept then would require a minimum number of space objects available in each altitude band. Inherently, this technique would require a larger initial population size $N$. As a part of this planned effort, we would seek to identify the number of space objects required.

We also looked at finding consistent solutions and discovered that this was a difficult prospect given our current formulation. Future work should address what parameterization the density correction equation should take in order to achieve a more consistent solution. Ideally we would like to incorporate angular parameterizations such as latitude and local apparent solar time. However, since the TLE data is available only at nodal crossing points, the observability of these parameters would be suspect.

# References


[1] Jacchia, L. G., "Revised Static Models of the Thermosphere and Exosphere with Empirical Temperature Profiles," Smithsonian Astrophysical Observatory SP-332, 1971.

[2] Jacchia, L. G., "Thermospheric Temperature, Density, and Composition: New models," Smithsonian Astrophysical Observatory SP-375, 1977.

[3] Voiskovskii, M. I. and Volkov, I. I., "Not spherical model of the upper atmosphere density," 1991.

[4] "Earths Upper Atmosphere Density Model for ballistic support of Flights of Artificial Earth Satellites. GOST 22721-77," Moscow, Publishing House of the Standards, 1978.

[5] Hedin, A. E. et al., "MSIS-86 Thermospheric Model," *Journal of Geophysical Research*, Vol. 92, No. 5, May 1987, pp. 4649–4662.

[6] Picone, J. M., Hedin, A. E., Drob, D. P., and Aikin, A. C., "NRLMSISE-00 empirical model of the atmosphere: Statistical comparisons and scientific issues," *Journal of Geophysical Research*, Vol. 107, No. A12, 2002, pp. 1468, doi:10.1029/2002JA009430.

[7] Barlier, F. et al., "A thermospheric model based on satellite drag data," *Ann. Geophys.*, , No. 34, 1978.

[8] Berger, C., Biancale, R., Ill, M., and Barlier, F., "Improvement of the empirical thermospheric model DTM: DTM4 a comparative revive of various temporal variations and prospects in space geodesy applications," *Journal of Geodesy*, , No. 72, 1998, pp. 161–178.

[9] Bowman, B. R., Tobiska, W. K., and Marcos, F. A., "A New Thermospheric Density Model JB2006 Using New Solar Indices," 2006 Astrodynamics Specialist Conference, AAS Paper 06-6166, Keystone, CO, August 21-24, 2006.

[10] Nazarenko, A. I., Cefola, P. J., and Yurasov, V., "Estimating Atmosphere Density Variations to Improve LEO Orbit Predicition Accuracy," AAS Paper 98-190, 1998.

[11] Cefola, P. J., Nazarenko, A. I., Proulx, R., and Yurasov, V., "Atmospheric Density Correction Using Two Line Element Sets as the Observation Data," Paper AAS 03-626 of the AAS/AIAA Astrodynamics

Specialist Conference, Big Sky, Montana, August 2003.

[12] Yurasov, V., Nazarenko, A. I., Cefola, P. J., and Proulx, R., "Near Real Time Corrections to the Atmospheric Density Model," 5th US/Russian Space Surveillance Workshop, St. Petersberg, Russia, September 2003.

[13] Yurasov, V., Nazarenko, A. I., Cefola, P. J., and Alfriend, K. T., "Results and Issues of Atmospheric Density Correction," Paper AAS 04-305 of the $14^{th}$ AAS/AIAA Space Flight Mechanics Conference, Maui, Hawaii, February 2004.

[14] Granholm, G. R., "Near-Real Time Atmospheric Density Model Correciton Using Space Catalog Data," Master's Thesis, Massachusetts Institute of Technology, June 2000, CSDL-T-1380.

[15] Bergstrom, S., "An Algorithm for Reducing Atmospheric Density Model Errors Using Satellite Observation Data in Real-Time," Master's Thesis, Massachusetts Institute of Technology, June 2002.

[16] Wilkins, M. P., Sabol, C. A., Cefola, P. J., and Alfriend, K. T., "Practical Challenges in Implementing Atmospheric Density Corrections to the NRLMSISE-00 Model," $16^{th}$ AAS/AIAA Space Flight Mechanics Conference, AAS Paper 06-170, Tampa, FL, January 22-26, 2006.

[17] Yurasov, V., Nazarenko, A. I., Cefola, P. J., and Alfriend, K. T., "Density Corrections for the NRLMSIS-00 Atmosphere Model," Paper AAS 05-168 of the $15^{th}$ AAS/AIAA Space Flight Mechanics Conference, Copper Mountain, Colorado, January 2005.

[18] Wilkins, M. P., Sabol, C. A., Cefola, P. J., and Alfriend, K. T., "Validation and Application of Corrections to the NRLMSISE-00 Atmospheric Density Model," $17^{th}$ AAS/AIAA Space Flight Mechanics Conference, AAS Paper 07-189, Sedona, AZ, Jan 28 – Feb 1, 2007.

[19] Scientific-Industrial Firm "NUCLON", "Atmosphere Density Variation Tracking, Phase III," Charles Stark Draper Laboratory, Inc., September 2003.

[20] Wilkins, M. P., Sabol, C. A., Cefola, P. J., and Alfriend, K. T., "Improving Dynamic Calibration of the Atmospherel," $17^{th}$ AAS/AIAA Space Flight Mechanics Conference, AAS Paper 07-185, Sedona, AZ, Jan 28 – Feb 1, 2007.

[21] Gorochov, Y. P. and Nazarenko, A. I., "Methodical Points in Building Models of the Fluctuation of the Atmosphere Parameters," *Astronomicheskii Sovet Akademii Nauk SSSR*, Vol. 80, 1982, A copy was obtained by the MIT Lincoln Laboratory Library in January 2004 from the CISTI Document Delivery Service and translated by MIT Aeronautics and Astronautics Department graduate student Kalina Galabova in February 2004.

[22] Scientific-Industrial Firm "NUCLON", "Atmospheric Density Tracking Studies," Charles Stark Draper Laboratory, Inc., CSDL-C-6505, August 1999.